Weak-light solitons and their active control in a parity-time-symmetric atomic system

Chao Hang and Guoxiang Huang

Weak-Light Solitons and Their Active Control in a Parity-Time Symmetric Atomic System

Chao Hang[1,2,*] and Guoxiang Huang[1,2,†]

[1]*State Key Laboratory of Precision Spectroscopy and Department of Physics,*

East China Normal University, Shanghai 200062, China

[2]*ECNU-NYU Joint Physics Research Institute at NYU-Shanghai, Shanghai 200062, China*

Abstract

We propose a realistic physical scheme to produce one-dimensional (1D) and 2D weak-light solitons in an atomic system with parity-time ($\mathcal{PT}$) symmetry. The system we suggest is a cold three-level atomic gas with two species and driven by a control and a probe laser fields. We show that by the interference of two Raman resonances highly adjustable probe-field refractive-index with $\mathcal{PT}$ symmetry in 1D and 2D can be realized. We further show that it is possible to produce various light solitons when the weak nonlinearity of the probe field is taken into account. Due to resonant character of the system, the light solitons obtained in 1D and 2D have extremely low light power (at the level of nanowatt). In addition, we demonstrate that the stability of these light solitons can be actively controlled via $\mathcal{PT}$ phase transition of the system.

_____

* chang@phy.ecnu.edu.cn

† gxhuang@phy.ecnu.edu.cn

I. INTRODUCTION

Non-Hermitian Hamiltonians can exhibit entirely real spectra provided they respect parity-time ($\mathcal{PT}$) symmetry [1–4]. Due to the similarity between Schrödinger equation and the Maxwell equation under paraxial approximation, optics provides a fertile ground where $\mathcal{PT}$-related concepts can be realized and experimentally tested [5, 6]. Since the complex, space-dependent refractive index of a medium, $n(x)$, plays the role of the optical potential, the $\mathcal{PT}$ condition implies that real part of the index $\mathrm{Re}[n(x)]$ must be even while the imaginary part of the index $\mathrm{Im}[n(x)]$, which may have the property of loss or gain, must be odd. That is to say, $\mathcal{PT}$ symmetry requires $n(x) = n(-x)^*$.

Due to the significant progress achieved in recent years by developing optical materials with adjustable refractive index, $\mathcal{PT}$-symmetric optical systems made of solid-state waveguides and fiber networks [7–10], multi-level atomic systems [11–15], and microcavities [16, 17] have been suggested or realized experimentally. Particularly, $\mathcal{PT}$-symmetric system based on atomic gas and laser fields [11–15] possesses unique advantages that it has the authentic $\mathcal{PT}$-symmetric refractive index, i.e., balanced gain and loss in the whole space, and can be actively controlled and precisely manipulated by changing the system parameters *in situ*. These advantages may be useful to the applications such as $\mathcal{PT}$-symmetric laser absorber [18], unidirectional invisibility [19], invisible cloak [20], and so on.

On the other hand, recently much attention has been paid to the light solitons formed in $\mathcal{PT}$-symmetric media. Various light solitons have been suggested in different types of $\mathcal{PT}$-symmetric models such as the nonlinear Schrödinger (NLS) equations with linear and/or nonlinear $\mathcal{PT}$-symmetric potentials [21–31], $\mathcal{PT}$-symmetric couplers [32, 33], $\chi^{(2)}$ systems with $\mathcal{PT}$-symmetric potentials [34], discrete NLS equations with $\mathcal{PT}$-symmetric lattices [35, 36], vector NLS equations with $\mathcal{PT}$-symmetric potentials [37], etc. Since a $\mathcal{PT}$-symmetric multi-level atomic system can be made highly nonlinear due to the existence of Raman resonances [14, 15], it allows incorporating the $\mathcal{PT}$ symmetry into a nonlinear system and may serve as a nice test bed for different types of light solitons by using low light intensity.

In this article, we propose a new, realistic physical scheme to produce one-dimensional (1D) and 2D weak-light solitons in a system with $\mathcal{PT}$ symmetry. The system we suggested is a cold three-level atomic gas with two species and driven by a control and a probe laser fields. We show that, by the interference of two Raman resonances, a highly adjustable, periodic

probe-field refractive index with $\mathcal{PT}$ symmetry in 1D and 2D can be realized. Different from the result in Ref. [11], the $\mathcal{PT}$-symmetric refractive index obtained here can be continuously tunable and only a weak Stark laser field is needed. We further show that it is possible to create 1D and 2D light solitons when the weak nonlinearity of the probe field is considered. Due to resonant character of the system, the light solitons obtained have extremely low light power (at the level of nanowatt). In addition, we demonstrate that the stability of these light solitons can be actively controlled via $\mathcal{PT}$ phase transition of the system.

The article is arranged as follows. In Sec. II, the physical model under study is described. Expressions of the linear and nonlinear optical susceptibilities are presented. In Sec. III, the formation and stability of light solitons in 1D $\mathcal{PT}$-symmetric potential is investigated, and the threshold power for generating these light solitons is estimated. In Sec. IV, the active control on the stability of the solitons via the $\mathcal{PT}$-symmetric phase transition is discussed. In Sec. V, the weak-light solitons in 2D $\mathcal{PT}$-symmetric potential is studied. In Sec. VI we summarize the main results obtained in this work.

II. MODEL

We start with the physical setting reported in [11], which consists of an atomic gas with two isotopes, ^{87}Rb (species 1) and ^{85}Rb isotopes (species 2), as shown in Fig. 1(a). The atoms are loaded into a cell at low temperature ($\sim \mu K$). Each isotope is represented by three-level configuration with two ground-state sublevels $|g, s\rangle$ and $|a, s\rangle$, and one excited state $|e, s\rangle$ ($s = 1, 2$ indicates the specie of the atoms). A weak pulsed probe field $\mathbf{E}_p$ and a strong continuous control field $\mathbf{E}_c$, propagating along the z-direction with wavenumbers k_p and k_c, couple ground-state sublevels $|g, s\rangle$ and $|a, s\rangle$ to excited level $|e, s\rangle$, respectively. For the mixture of rubidium isotopes we assign $|g, s\rangle = |5S_{1/2}, F = 1\rangle$, $|a, s\rangle = |5S_{1/2}, F = 2\rangle$, and $|e, s\rangle = |5P_{1/2}, F = 1\rangle$. The half Rabi frequencies of the probe and control fields are $\Omega_p = |\mathbf{e}_p \cdot \mathbf{p}_{\mathrm{eg}}| E_p / (2\hbar)$ and $\Omega_c = |\mathbf{e}_c \cdot \mathbf{p}_{\mathrm{ea}}| E_c / (2\hbar)$, respectively. Here $\mathbf{p}_{\mathrm{eg}}$ ($\mathbf{p}_{\mathrm{ea}}$) represents electric dipole matrix element associated with transition from $|e, s\rangle$ to $|g, s\rangle$ ($|e, s\rangle$ to $|a, s\rangle$), which is assumed to be approximately equal for both isotopes. $\mathbf{e}_p$ and $\mathbf{e}_c$ (E_p and E_c) are, respectively, the polarization unit vectors (envelopes) of the probe and control fields.

Under electric-dipole and rotating-wave approximations, the Hamiltonian of the system
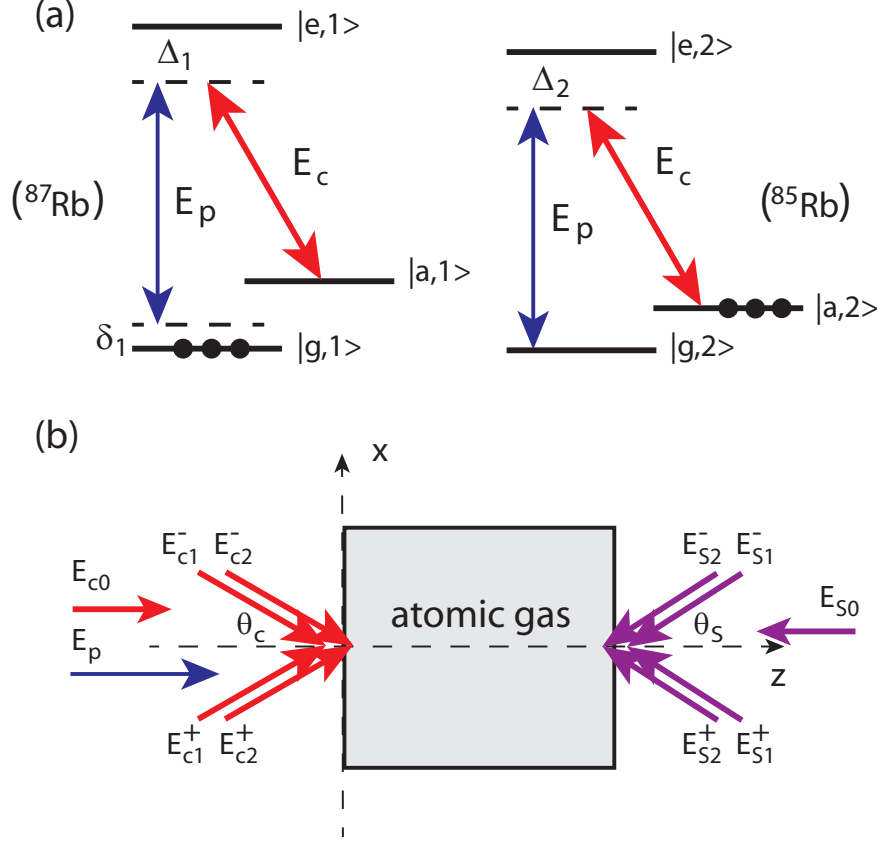
FIG. 1: (Color online) (a) Energy-level diagram and Raman resonance scheme of the mixture of two three-level Λ systems. E_p: probe field (with the frequency ω_p and wavevector k_p). E_c: control field (with the frequency ω_c and wavevector k_c). Δ_s $(s = 1, 2)$: one-photon detunings; δ_1: two-photon detunings. The black points indicate the levels initially populated. (b) Possible experimental arrangement. The control (Stark) field E_c (E_S) consists of a z-direction laser beam (i.e. E_{c0} (E_{S0})) and two pairs of laser beams (i.e. $E_{cj}^{\pm}$ $(E_{Sj}^{\pm})$ $(j = 1, 2)$) with cross angle θ_c (θ_S).

in interaction picture reads

$$\hat{H}_{\text{int}} = \sum_{s=1}^{2} \{\hbar[\delta_s |a, s\rangle\langle a, s| + (\Delta_s + \delta_s)|e, s\rangle\langle e, s|]$$
$$- \hbar(\Omega_p |e, s\rangle\langle g, s| + \Omega_s |e, s\rangle\langle a, s| + \text{H.c.})\}, \quad (1)$$

where $\Delta_s = \omega_e^s - \omega_a^s - \omega_c$ is the one-photon detuning and $\delta_s = \omega_a^s - \omega_g^s - (\omega_p - \omega_c)$ is the two-photon detuning, with ω_l^s $(l = g, a, e)$ the eigenfrequency of the level $|l, s\rangle$.

The motion of atoms is governed by the master equation for the atomic density matrix

[38]:

$$\frac{\partial \rho}{\partial t} = \frac{1}{i\hbar}[\hat{H}_{\rm int}, \rho] + \frac{\Gamma_{eg}}{2}\sum_{s=1}^{2}(2\hat{\sigma}_{ge}^s\rho\hat{\sigma}_{eg}^s - \hat{\sigma}_{ee}^s\rho - \rho\hat{\sigma}_{ee}^s) + \frac{\Gamma_{ea}}{2}\sum_{s=1}^{2}(2\hat{\sigma}_{ae}^s\rho\hat{\sigma}_{ea}^s - \hat{\sigma}_{ee}^s\rho - \rho\hat{\sigma}_{ee}^s)$$

$$+ \frac{\gamma_{a,\rm deph}}{2}\sum_{s=1}^{2}(2\hat{\sigma}_{aa}^s\rho\hat{\sigma}_{aa}^s - \hat{\sigma}_{aa}^s\rho - \rho\hat{\sigma}_{aa}^s) + \frac{\gamma_{e,\rm deph}}{2}\sum_{s=1}^{2}(2\hat{\sigma}_{ee}^s\rho\hat{\sigma}_{ee}^s - \hat{\sigma}_{ee}^s\rho - \rho\hat{\sigma}_{ee}^s), \qquad (2)$$

where $\hat{\sigma}_{jk}^s = |j,s\rangle\langle k,s|$ is the atomic projection operator (j, $k = g$, a, e). Γ_{ea} and Γ_{eg} are the spontaneous-emission decay rates from the excited state $|e,s\rangle$ to two ground-state sublevels $|a,s\rangle$ and $|g,s\rangle$, respectively. They are assumed to be approximately equal for both isotopes. The decay rate from $|a,s\rangle$ to $|g,s\rangle$ is about four orders smaller than Γ_{eg} or Γ_{ea}, and hence can be safely neglected. We have also introduced the energy-conserving dephasing processes with rates $\gamma_{a,\rm deph}$ and $\gamma_{e,\rm deph}$. Thus, the coherence decay rates are defined as $\gamma_{eg} = (\Gamma_{eg} + \Gamma_{ea} + \gamma_{e,\rm deph})/2$, $\gamma_{ea} = (\Gamma_{eg} + \Gamma_{ea} + \gamma_{e,\rm deph} + \gamma_{a,\rm deph})/2$, and $\gamma_{ag} = \gamma_{a,\rm deph}/2$.

As the isotopes are loaded in a cell at low temperature, the spontaneous-emission decay rates are given by $\Gamma_{eg} \approx \Gamma_{ea} \approx \pi \times 5.75$ MHz for Rubidium atoms [39], while the dephasing rates can be very small. In addition, for simplicity the two-photon detuning of the second isotope is taken as zero, i.e. $\delta_2 = 0$, which can be achieved by tuning the frequency of the probe field ω_p and the elimination of the Doppler broadening due to low temperature.

Taking into account above considerations, the Bloch equation describing the motion of atoms is given by

$$i\dot{\rho}_{gg}^s = i\Gamma_{eg}\rho_{ee}^s - \Omega_p^*\rho_{eg}^s + \Omega_p\rho_{eg}^{s*}, \qquad (3a)$$

$$i\dot{\rho}_{aa}^s = i\Gamma_{ea}\rho_{ee}^s - \Omega_c^*\rho_{ea}^s + \Omega_c\rho_{ea}^{s*}, \qquad (3b)$$

$$i\dot{\rho}_{ee}^s = -i(\Gamma_{eg} + \Gamma_{ea})\rho_{ee}^s + \Omega_p^*\rho_{eg}^s - \Omega_p\rho_{eg}^{s*} + \Omega_c^*\rho_{ea}^s - \Omega_c\rho_{ea}^{s*}, \qquad (3c)$$

$$i\dot{\rho}_{ag}^s = -d_{ag}^s\rho_{ag}^s + \Omega_p\rho_{ea}^{s*} - \Omega_c^*\rho_{eg}^s, \qquad (3d)$$

$$i\dot{\rho}_{eg}^s = -d_{eg}^s\rho_{eg}^s + \Omega_p(\rho_{ee}^s - \rho_{gg}^s) - \Omega_c\rho_{ag}^s, \qquad (3e)$$

$$i\dot{\rho}_{ea}^s = -d_{ea}^s\rho_{ea}^s + \Omega_c(\rho_{ee}^s - \rho_{aa}^s) - \Omega_p\rho_{ag}^{s*}, \qquad (3f)$$

where the overdots stand for the time derivative and we have defined $d_{ag}^s = \delta_{s,1}\delta_1 + i\gamma_{ag}$ ($\delta_{i,j} = 1$ for $i = j$; $\delta_{i,j} = 0$ for $i \neq j$), $d_{ea}^s = -\Delta_s + i\gamma_{ea}$, and $d_{eg}^s = \delta_{s,1}\delta_1 - \Delta_s + i\gamma_{eg}$, with $\delta_1 \ll \Delta_s$. Note that we are interested in the case where a semiclassical theory can be applied, i.e. both control and probe laser fields contain a large number of photons and hence can be treated as classical fields.

The susceptibility of the probe field is defined by $\chi_p = p_{eg}^2(N_1\rho_{eg}^1 + N_2\rho_{eg}^2)/(\epsilon_0\hbar\Omega_p)$, where N_s is the density of the s-th isotope and the coherence ρ_{eg}^s can be computed from the Bloch equation (3). Using the smallness of the intensity of the probe field, i.e., $|\Omega_p/\Omega_c| \ll 1$ ($|\Omega_p/\Omega_c| \approx 10^{-3/2}$, see the discussion below), we employ the expansions $\rho_{jk}^s = \sum_{m=0}^{\infty}\rho_{jk,m}^s$ ($j,k = g,a,e$), where $\rho_{jk,m}^s$ is of order of $|\Omega_p/\Omega_c|^m$. Substituting the expansions into the Bloch equation (3) and neglecting the derivative with respect to time (we are interested in stationary states), Eqs. (3) in the leading order are solved by $\rho_{gg,0}^1 = \rho_{aa,0}^2 = 1$ and $\rho_{ea,0}^2 = -\Omega_c/d_{ea}^2$, with other leading elements of the density matrix being zero. In higher orders, we obtain the recurrent equations:

$$\begin{pmatrix} d_{ag}^s & \Omega_c^* \\ \Omega_c & d_{eg}^s \end{pmatrix}\begin{pmatrix} \rho_{ag,m}^s \\ \rho_{eg,m}^s \end{pmatrix} = \Omega_p\begin{pmatrix} \rho_{ea,m-1}^{s*} \\ \rho_{ee,m-1}^s - \rho_{gg,m-1}^s \end{pmatrix}, \tag{4a}$$

$$\begin{pmatrix} i\Gamma_{eg} & i\Gamma_{eg} & 0 & 0 \\ i\Gamma_{ea} & i\Gamma_{ea} & \Omega_c^* & -\Omega_c \\ \Omega_c & 2\Omega_c & d_{ea}^s & 0 \\ -\Omega_c^* & -2\Omega_c^* & 0 & -d_{ea}^{s*} \end{pmatrix}\begin{pmatrix} \rho_{gg,m}^s \\ \rho_{aa,m}^s \\ \rho_{ea,m}^s \\ \rho_{ae,m}^s \end{pmatrix} = \mathbf{M}_{m-1}, \tag{4b}$$

with $\mathbf{M}_m = (\Omega_p\rho_{eg,m}^{s*} - \Omega_p^*\rho_{eg,m}^s, 0, -\Omega_p\rho_{ag,m}^{s*}, \Omega_p^*\rho_{ag,m}^s)^T$. When obtaining Eq. (4) the conservation relation $\rho_{ee,m}^s = \delta_{0,m} - \rho_{gg,m}^s - \rho_{aa,m}^s$ is used.

The expression of coherence ρ_{eg}^s up to the third order ($|\Omega_p/\Omega_c|^3$-order) was computed in Refs. [11]. The result showed that the probe-field susceptibility has the form $\chi_p \approx \chi_{p,1} + |\Omega_p/\Omega_c|^2\chi_{p,3}$, where the first- and third-order susceptibilities are respectively given by

$$\chi_{p,1} = \frac{p_{eg}^2}{\epsilon_0\hbar}(N_1 D_1 + N_2 D_2), \tag{5}$$

$$\chi_{p,3} \approx -\frac{p_{eg}^2}{\epsilon_0\hbar}\left\{\frac{N_1}{\Delta_1} + N_1\frac{4|\Omega_c|^2 - 3\delta_1^2 + i\delta\Gamma}{\Delta_1^2\delta} + \frac{3N_2}{\Delta_2} - iN_2\frac{\Gamma}{\Delta_2^2}\right\}, \tag{6}$$

with $D_1 = \delta_1/[\delta_1(\delta_1 + \Delta_1 - i\Gamma) - |\Omega_c|^2]$ and $D_2 = 1/(\Delta_2 + i\Gamma)$. Here we have assumed that $\Gamma_{ea} \approx \Gamma_{eg} = \Gamma$ within the required accuracy. In addition, we have used the scalings $\Delta_s \sim |\Omega_p/\Omega_c|^{-1/2}\Gamma$ and $\Omega_c \sim \delta_1 \sim \Gamma$ for obtaining expression (6), which correspond to a realistic choice of the system parameters given below.

The spatial distribution of the $\mathcal{PT}$-symmetric probe-field susceptibility, $\chi_p(x) = \chi_p^*(-x)$ [and hence the $\mathcal{PT}$-symmetric refractive index $n(x) = \sqrt{1 + \chi_p(x)} = n^*(-x)$], is obtained by applying a far-detuned laser field (i.e., the Stark field), $E_S(x)\cos(\omega_S t)$ [11], which induces energy shifts of levels $|j,s\rangle$, i.e. $\Delta E_{j,S}(x) = -\alpha_j E_S^2(x)/4$ (here α_j is the scalar polarizability).

In addition, the control field is assumed to be x-dependent, i.e. $\Omega_c = \Omega_c(x)$. For the selected levels of rubidium atoms, $\alpha_e - \alpha_g \approx 2\pi\hbar \cdot 0.1223$ Hz(cm/V)^2 and $\alpha_g \approx \alpha_a$ [39]. That means the difference of the Stark shifts between the ground-state sublevels is negligible, i.e. the two-photon detuning δ_1 is not affected by the Stark field, while the one-photon detunings become x-dependent, $\Delta_s(x) = \Delta_s - (\alpha_e - \alpha_g)E_S^2(x)/(4\hbar)$. Note that the characteristic scale of the $\Delta_s(x)$ modulation is comparable to the Stark-field wavelength λ_S.

In what follows, we focus on the values of detunings: $\Delta_1 = 8\,\Gamma$, $\Delta_2 = 8.72\,\Gamma$, and $\delta_1 = 1.81\,\Gamma$. The electric dipole matrix element is $p_{eg} = 2.5377 \times 10^{-27}$ C·cm [39]. The atomic densities of the first and second isotopes are $N_1 \approx 2.23 \times 10^{14}$ cm^{-3} and $N_2 \approx 4.81 \times 10^{14}$ cm^{-3}, respectively.

The equation of motion for the probe-field Rabi frequency Ω_p can be obtained by using the Maxwell equation $\nabla^2 \mathbf{E}_p - (1/c^2)\partial^2 \mathbf{E}_p/\partial t^2 = [1/(\varepsilon_0 c^2)]\partial^2 \mathbf{P}/\partial t^2$, where the polarization intensity of the probe field is given by $\mathbf{P} = \sum_{s=1}^{2} N_s \mathbf{p}_{eg,s}\sigma_{eg,s}e^{i(k_p z - \omega_p t)} + $ c.c.. Thus, under paraxial and slowly-varying envelope approximations, Ω_p satisfies

$$i\frac{k_p^2}{k_S^2}\frac{\partial \Omega_p}{\partial \zeta} + \frac{1}{2}\frac{\partial^2 \Omega_p}{\partial \xi^2} + \frac{k_p^2}{2k_S^2}\chi_p(\xi)\Omega_p = 0. \tag{7}$$

where $\zeta = k_p z$ and $\xi = k_S x$ ($k_S = 2\pi/\lambda_S$). The term $\frac{1}{2}\frac{\partial^2 \Omega_p}{\partial \xi^2}$ describes the diffraction of the probe beam in the x direction, however, the diffraction in the y direction is neglected. This can be realized by choosing the incident probe field more focused in the x direction than that in the y direction.

The first-order susceptibility can be expressed as $\chi_{p,1}(\xi) = \bar{\chi}_{p,1} + \tilde{\chi}_{p,1}(\xi)$, where $\bar{\chi}_{p,1}$ and $\tilde{\chi}_{p,1}(\xi)$ are, respectively, the constant and modulated parts of $\chi_{p,1}(\xi)$. With the given parameters, the modulated part $\tilde{\chi}_{p,1}(\xi)$ is two orders smaller than the homogeneous part $\bar{\chi}_{p,1}$, i.e. $|\tilde{\chi}_{p,1}(\xi)/\bar{\chi}_{p,1}| \sim |\Omega_p/\Omega_c|^2$. Using the transformation $\Omega_p(\xi, \zeta) = u(\xi)U_0 e^{ib\zeta}$ (b is the propagation constant; U_0 is the typical Rabi frequency) and preserving the terms up to the third order ($\sim |\Omega_p/\Omega_c|^3$-order), the propagation equation (7) can be written into the equation:

$$\frac{\partial^2 u}{\partial \xi^2} + V(\xi)u + G(\xi)|u|^2 u = \beta u, \tag{8}$$

where $V(\xi) = \frac{k_p^2}{k_S^2}\tilde{\chi}_{p,1}(\xi)$ represents the optical potential, $G(\xi) = \frac{k_p^2 U_0^2}{k_S^2 |\Omega_c|^2}\chi_{p,3}(\xi)$ is the coefficient characterizing the magnitude of the nonlinearity, and the eigenvalue $\beta = \frac{k_p^2}{k_S^2}(2b - \bar{\chi}_{p,1})$.

The third-order probe-field susceptibility $\chi_{p,3}$ is given by Eq. (6), which can also be separated by a constant part and a space-modulated part. Although the space-modulated

7

part generally violates the $\mathcal{PT}$-symmetry, it is however much smaller than the constant part. Consequently, under the required accuracy the space-modulated part can be safely neglected. In addition, the imaginary part of $\chi_{p,3}$ is much smaller than its real part and can also be neglected.

For the parameters given above we obtain $\chi_{p,3} \approx -16.99$, which results in $G \approx -1$ after taking $U_0 = 0.08\Gamma$ and $k_S = 0.13 k_p$ (i.e., $\lambda_S \approx 5$ μm for $\lambda_p \approx 658$ nm). Notice that the wavelength of Stark field is inside the mid-infrared spectral range, which can be generated by a quantum cascade laser working in room temperature and continuous wave operation [40, 41]. Since the sign of G is negative, the system possesses a defocusing Kerr nonlinearity. We should emphasize that very weak probe-field intensity is needed for obtaining such nonlinearity in the present system (see the discussion below). This is because the third-order susceptibility is largely enhanced due to the existence of two nearly resonant Raman transitions. This is very different from any passive optical materials where intensive laser fields are usually required for obtaining enough nonlinearity to balance the dispersion or diffraction of the system.

III. WEAK-LIGHT SOLITONS IN 1D $\mathcal{PT}$-SYMMETRIC POTENTIAL

Since for the present active system the physical parameters are tunable, we can obtain various potentials $V(\xi)$ with $\mathcal{PT}$-symmetry [11]. For illustration purpose, we first consider the possibility of weak-light solitons and study their stability for the 1D periodic $\mathcal{PT}$-symmetric potential

$$V(\xi) = V_0 \cos^2(\xi) + iW_0 \sin(2\xi). \tag{9}$$

Generally, the band structure of a complex periodic potential is complex. For a $\mathcal{PT}$-symmetric periodic potential, however, the band diagram can be entirely real as long as the system operates below the $\mathcal{PT}$ phase transition point. For the potential (9), purely real bands are possible in the range of $0 \le W_0/V_0 < 1/2$ [21].

In our system, the $\mathcal{PT}$-symmetric potential (9) can be realized by choosing

$$\chi_{p,1}(\xi) = 0.460 - 10^{-3}[V_0 \cos^2(\xi) + iW_0 \sin(2\xi)]. \tag{10}$$

This gives the order of magnitude of the small parameter $|\Omega_p/\Omega_c|^2 \sim 10^{-3}$ and hence defines the accuracy of the expansion. The susceptibility (10) can be created by using the following

control and Stark fields shaped as

$$\Omega_c(\xi)/\Gamma \approx 2.553 - 0.002V_0 \sin^2(\xi) - 0.032W_0 \sin(2\xi), \tag{11}$$

$$E_S(\xi)/E_0 \approx 0.97 + 0.008V_0 \sin^2(\xi) + 0.021W_0 \sin(2\xi), \tag{12}$$

with $E_0 = 10^4$ V/cm^{-2} (more details are given in Appendix A). Note that in expressions (11) and (12) we have preserved undetermined parameters V_0 and W_0, which allows the possibility of tuning the potential in a continuous way.

The experimental realization of the control and Stark fields Eqs. (11) and (12) can be realized in the following way. Assume the control field consists of a z-direction laser beam with the form $\mathbf{E}_{c0} = \mathbf{e}_y E_{c0} e^{ik_c z - i\omega_c t}$, and two pairs of laser beams with the forms $\mathbf{E}_{cj}^{\pm} = \mathbf{e}_y (E_{cj}/2) e^{ik_c(\pm x \sin\theta_c + z\cos\theta_c) - i\omega_c t \pm i\phi_j}$ ($j = 1, 2$) (θ_c is cross angle which is the same for all the pairs), as shown in Fig. 1(b). Here E_{cj} and ϕ_j are, respectively, the amplitudes and phases of the j-th pair of laser beams. If θ_c is very small, i.e. $\sin\theta_c \ll 1$ and $\cos\theta_c \approx 1$, the control field can be written as $\mathbf{E}_c = \mathbf{e}_y e^{ik_c z - i\omega_c t}[E_{c0} + E_{c1}\cos(xk_c\sin\theta_c + \phi_1) + E_{c2}\cos(xk_c\sin\theta_c + \phi_2)]$, which further leads to $\Omega_c(x) = \Omega_{c0} + \Omega_{c1}\cos(xk_c\sin\theta_c + \phi_1) + \Omega_{c2}\cos(xk_c\sin\theta_c + \phi_2)$, where $\Omega_{c0} = |\mathbf{e}_y \cdot \mathbf{p}_{ea}|E_{c0}/(2\hbar)$ and $\Omega_{cj} = |\mathbf{e}_y \cdot \mathbf{p}_{ea}|E_{cj}/(2\hbar)$. Thus, if taking

$$\Omega_{c0} = (2.553 - 0.001V_0)\Gamma, \quad \Omega_{c1} = 0.001V_0\Gamma, \quad \Omega_{c2} = 0.032W_0\Gamma, \tag{13}$$

with $\sin\theta_c = 2k_S/k_c$, $\phi_1 = 0$, and $\phi_2 = \pi/2$, we obtain the control field (11).

The Stark field (12) can also be realized by using the same method. We assume the Stark field consists a z-direction laser beam, $\mathbf{E}_{S0} = \mathbf{e}_y E_{S0} e^{-ik_S z - i\omega_S t}$, and two pairs of laser beams, $\mathbf{E}_{Sj}^{\pm} = \mathbf{e}_y (E_{Sj}/2) e^{-ik_S(\mp x\sin\theta_S + z\cos\theta_S) - i\omega_S t \pm i\phi_j}$, as shown in Fig. 1(c). If the cross angle θ_S is very small, the Stark field can be written as $\mathbf{E}_S = \mathbf{e}_y e^{-ik_S z - i\omega_S t}[E_{S0} + E_{S1}\cos(xk_S\sin\theta_S + \phi_1) + E_{cS}\cos(xk_S\sin\theta_S + \phi_2)]$. Thus, when taking

$$E_{S0} = (0.97 + 0.004V_0)E_0, \quad E_{S1} = 0.004V_0 E_0, \quad E_{S2} = 0.021W_0 E_0, \tag{14}$$

with $\theta_S = \theta_c$, $\phi_1 = -\pi$, $\phi_2 = -\pi/2$, we obtain the Stark field (12).

From Eq. (11) and Eq. (12) we can estimate the powers required for generating the control and Stark fields. The control-field amplitude $E_c \approx 2.7$ V cm^{-1} ($\Omega_c \approx 4.6 \times 10^7$ Hz), while the amplitude of the Stark field $E_S \approx 97$ V cm^{-1}. Being focused into a spot with radius ≈ 0.1 mm, this requires laser power ≈ 3.9 mW. *Thus the laser power of the Stark field required*

9

here is much smaller than that required in Ref. [11]. This is because a cold atomic system is used here.

In Fig. 2(a) we plot the real and imaginary parts of the refractive index $n(\xi)$ as functions of $k_S x/\pi$ for $V_0 = 3.0$ and $W_0 = 0.75$, which is below the $\mathcal{PT}$ phase transition point. The control and Stark fields required for the $\mathcal{PT}$-symmetric refractive index as functions of $k_S x/\pi$ are plotted in Fig. 2(b). In order to estimate the accuracy of the refractive-index $\mathcal{PT}$ symmetry, we define the error function $\nu(\xi) = n(\xi) - n^*(-\xi)$. Its real and imaginary parts are of order of 10^{-7} and 10^{-6}, respectively, i.e. a very high accuracy for the $\mathcal{PT}$ symmetry is obtained.

We also show the associated band-gap structure for various values of the potential parameter W_0, by taking $W_0 = 0.75$ (below the $\mathcal{PT}$ phase transition point), 1.5 (on the $\mathcal{PT}$ transition point), and 2.25 (above the $\mathcal{PT}$ phase transition point). The real part of the "energy" band (i.e. $\text{Re}(\beta)$) as a function of lattice momentum q is plotted in Fig. 2(c). One sees that as W_0/V_0 increases the band gap becomes narrower and two bands become merged when crossing the critical transition value $W_0/V_0 = 1/2$. The imaginary part of the "energy" band (i.e. $\text{Im}(\beta)$) as a function of q is plotted in Fig. 2(d) for $V_0 = 3.0$ and $W_0 = 2.25$. In particular, $\text{Im}(\beta)$ is zero for all q for $W_0 = 0.75$ and 1.5.

With the band-gap structure obtained above, we seek the soliton solutions of Eq. (8) for the given complex potential Eq. (9) and for the nonlinear coefficient $G = -1$. It is known that self-defocusing nonlinearity combined with a real periodic potential can support stable gap solitons of bright type [42]. Thus we anticipate that the conclusion is still valid for a periodic potential with $\mathcal{PT}$ symmetry if it works below the $\mathcal{PT}$-symmetric phase transition point (i.e. without the $\mathcal{PT}$-symmetry breaking).

We have obtained a family of nonlinear localized solutions numerically for $W_0 = 0.75$. Since $W_0/V_0 = 0.25$, i.e. below the $\mathcal{PT}$ transition point, the linear eigenvalue problem has purely real spectrum (i.e. β is real) with eigenvalues located within the first band gap $-0.1 < \beta < 1.2$ (gap soliton). The real and imaginary parts of gap-soliton amplitude (i.e. $\text{Re}(\Omega_p)$ and $\text{Im}(\Omega_p)$) as a functions of $k_s x/\pi$ are shown in Fig. 3(a) for $\beta = 0.5$. The evolution of the gap soliton, after adding random noises on both amplitude and phase to initial condition, is given in Fig. 3(b), indicating that the soliton is fairly stable.

In comparison to the stable gap soliton described in Fig. 3(a) and Fig. 3(b), we have also obtained nonlinear localized structures for β located outside the band gap. Shown in
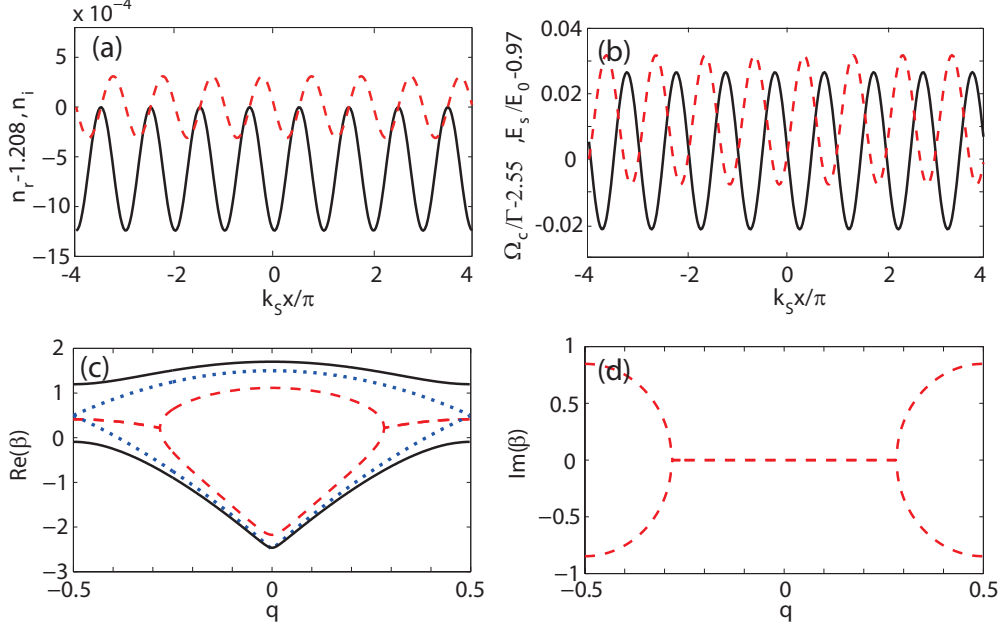
10

FIG. 2: (Color online) (a) Real (solid line) and imaginary (dashed line) parts of the refractive index $n(\xi)-1.208$ as functions of $k_S x/\pi$. (b) Control field $\Omega_c(\xi)/\Gamma-2.55$ (solid line) and Stark field $E_S(\xi)/E_0-0.97$ (dashed line) as functions of $k_S x/\pi$, required for the refractive index (a). (c) Re(β) as a function of q for $V_0 = 3.0$ and $W_0 = 0.75$ (solid lines), 1.5 (dotted lines), and 2.25 (dashed lines). (d) Im(β) as a function of lattice momentum q for $V_0 = 3.0$ and $W_0 = 2.25$. Im(β) is zero for all q for $W_0 = 0.75$ and 1.5.

Fig. 3(c) is the real and imaginary parts of such a solution for $\beta = 1.3$, which is within the second "energy" band. Its evolution is given in Fig. 3(d), indicating that it is highly unstable. This can be understood because in this case the potential cannot balance the defocusing nonlinearity.

The threshold of the optical power P_{th} for generating the stable soliton described in Fig. 3(a) and Fig. 3(b) can be estimated by using the Poynting's vector. Taking the beam radius ≈ 0.1 mm, we obtain

$$P_{th} \approx 3.7\,\text{nW}. \tag{15}$$

Thus, very low input power is needed to generate such light solitons in the present system.

IV. CONTROL OF STABILITY OF THE WEAK-LIGHT SOLITONS

In the last section, based on a realistic atomic system we have constructed nonlinear physical model with a 1D periodic complex potential with $\mathcal{PT}$ symmetry and with a defocusing
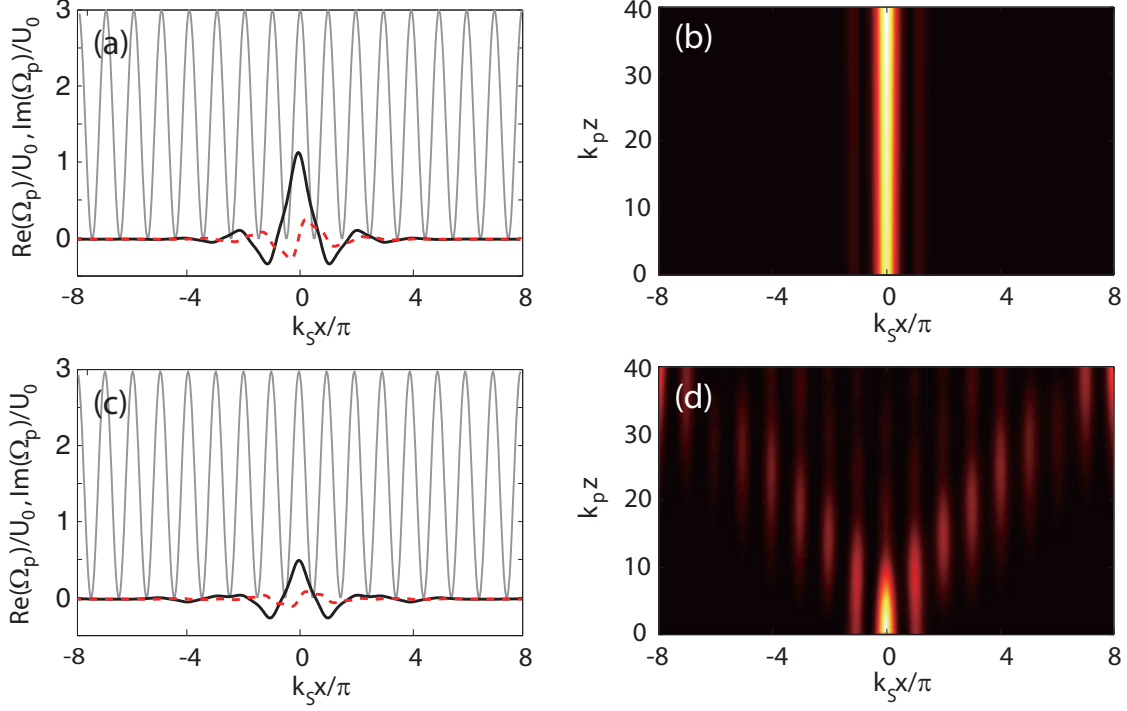
11

FIG. 3: (Color online) (a) Real part (Re(Ω_p); solid line) and imaginary part (Im(Ω_p); dashed line) of the stable gap-soliton as functions of $k_s x/\pi$ for $\beta = 0.5$. (b) Stable propagation of the gap soliton in the x-z plane. (c) Re(Ω_p) (solid line) and Im(Ω_p) (dashed line) for unstable soliton by taking $\beta = 1.3$ located within the second "energy" band. (d) Evolution of the unstable solution. The gray curves in (a) and (c) are the real part of the lattice.

Kerr nonlinearity. We have also shown that a weak-light bright soliton is indeed possible to be produced in such system and such soliton is stable (unstable) if its propagation constant β is located inside (outside) the first band gap. An interesting problem deserves to be explored is what will happen for the evolution of the soliton when the system passes through the $\mathcal{PT}$ phase transition point. Because our system is an active one, we can manipulate the system parameters to make the system work below and above the $\mathcal{PT}$ phase transition point, so as to realize an active control of soliton stability.

The control upon the state of $\mathcal{PT}$ symmetry of our system can be realized in many ways. One is to change the relative amplitude of the imaginary part of the $\mathcal{PT}$ potential by continuously tuning W_0 while keeping V_0 fixed.

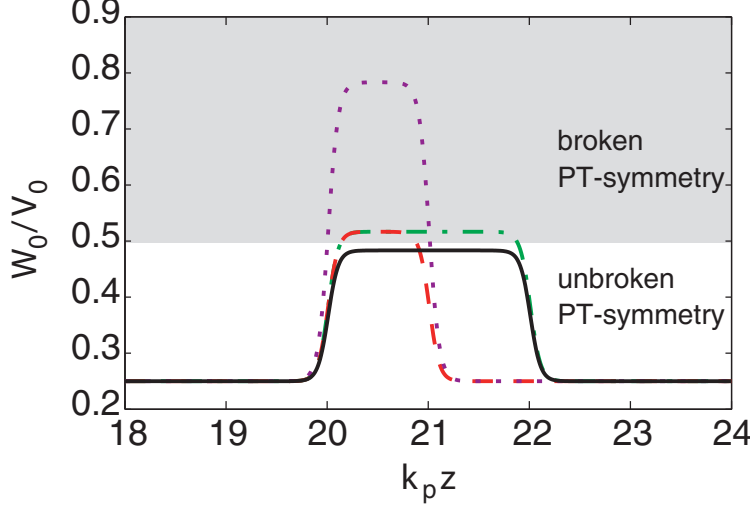As an example, we focus on the case that $V_0 = 3.0$ and W_0 is a z-dependent function

12

FIG. 4: (Color online) W_0/V_0 as a function of $k_p z$ for $(W_1, Z_1, Z_2) = (0.7, 20, 22)$ (black solid line), $(0.8, 20, 22)$ (green dashed-dotted line), $(0.8, 20, 21)$ (red dashed line), and $(1.6, 20, 21)$ (purple dotted line), respectively. The white (gray) domain is the one where the system works below (above) the $\mathcal{PT}$ phase transition. The boundary between the white and gray regions (i.e. $W_0/V_0 = 0.5$) corresponds to the $\mathcal{PT}$ phase transition point.

modeled by the combination of two hyperbolic tangent functions with the form

$$W_0(\zeta)/V_0 = 0.25 + \frac{W_1}{6}\{\tanh[10(\zeta - Z_1)] - \tanh[10(\zeta - Z_2)]\}, \tag{16}$$

which can be experimentally achieved by choosing the control and Stark fields with $\Omega_{c0} = 2.55\Gamma$, $\Omega_{c1} = 0.003\Gamma$, $E_{S0} = 0.982E_0$, $E_{S1} = 0.012E_0$, and

$$\Omega_{c2}/\Gamma = 0.024 + 0.016W_1\{\tanh[10(\zeta - Z_1)] - \tanh[10(\zeta - Z_2)]\}, \tag{17}$$

$$E_{S2}/E_0 = 0.016 + 0.011W_1\{\tanh[10(\zeta - Z_1)] - \tanh[10(\zeta - Z_2)]\}. \tag{18}$$

From Eq. (16) we see that the value of W_0/V_0 changes from 0.25 to $0.25 + W_1/3$ at around $\zeta = Z_1$, and changes back to 0.25 at around $\zeta = Z_2$. The system works below the $\mathcal{PT}$ phase transition point in the range $Z_1 < \zeta < Z_2$ if $W_1 < 0.75$ (i.e. $W_0/V_0 < 1/2$), and works above the $\mathcal{PT}$ phase transition point in the range $Z_1 < \zeta < Z_2$ if $W_1 > 0.75$ (i.e. $W_0/V_0 > 1/2$).

Fig. 4 shows W_0/V_0 as a function of $k_p z$ for $(W_1, Z_1, Z_2) = (0.7, 20, 22)$ (black solid line), $(0.8, 20, 22)$ (green dashed-dotted line), $(0.8, 20, 21)$ (red dashed line), and $(1.6, 20, 21)$ (purple dotted line), respectively. The white (gray) domain is the one in which the system works below (above) the $\mathcal{PT}$ phase transition. The boundary between the white and gray

regions (i.e. $W_0/V_0 = 0.5$) corresponds to the $\mathcal{PT}$ phase transition point. We see that for the case $(W_1, Z_1, Z_2) = (0.7, 20, 22)$ (black solid line), the system works below the $\mathcal{PT}$ phase transition point for all values of z; for the cases $(W_1, Z_1, Z_2) = (0.8, 20, 22)$ (green dashed-dotted line), $(0.8, 20, 21)$ (red dashed line), and $(1.6, 20, 21)$ (purple dotted line), the system works above the $\mathcal{PT}$ phase transition point for $Z_1 < k_p z < Z_2$ but below the $\mathcal{PT}$ phase transition point otherwise.

The propagation of a weak-light soliton in the x-z plane below and above the $\mathcal{PT}$ phase transition point is shown in Fig. 5. The initial condition is taken as the soliton solution given in Fig. 3(a). Illustrated in Fig. 5(a) is the result for $(W_1, Z_1, Z_2) = (0.7, 20, 22)$, which corresponds to the case of black solid line in Fig. 4 (i.e. the system works below the $\mathcal{PT}$ phase transition point for all values of z). We see that in this case the soliton is fairly stable during propagation.

Fig. 5(b) shows the evolution result for $(W_1, Z_1, Z_2) = (0.8, 20, 22)$ (i.e. the case of the green dashed-dotted line in Fig. 4). This case is obtained by lifting the values of W_0/V_0 in the region $Z_1 < k_p z < Z_2$ from the case $(W_1, Z_1, Z_2) = (0.7, 20, 22)$ (i.e. the black solid line in Fig. 4). We see that the soliton is stable in the region $k_p z < 20$, but it becomes unstable for $k_p z > 20$. It seems that the loss of the stability of the soliton for $k_p z > 20$ is due to the existence of a region (i.e. $20 < k_p z < 22$) where the system works above the $\mathcal{PT}$ phase transition point.

Interestingly, the instability of the soliton can be controlled and even be effectively suppressed by reducing the size of the region $Z_1 < k_p z < Z_2$. In Fig. 5(c) we show the soliton evolution for $(W_1, Z_1, Z_2) = (0.8, 20, 21)$ (the case of the red dashed line in Fig. 4). We see that the soliton is basically stable during propagation for nearly all z, although the system works above the $\mathcal{PT}$ transition point in $20 < k_p z < 21$.

However, when fixing $Z_1 = 20$ and $Z_2 = 21$ but increasing W_1 from 0.8 to 1.6 (i.e. in Fig. 4 the red dashed line is changed into the purple dotted line), we find that the soliton becomes unstable again, see Fig. 5(d). The instability of the soliton is induced by the deeper $\mathcal{PT}$-symmetry breaking.

From the results displayed in Fig. 5, we see that it is indeed possible to realize an active control on a series of stability-instability transitions of the weak-light soliton in the present $\mathcal{PT}$- symmetric system through actively manipulating the system parameters V_0, W_0, W_1, Z_1, and Z_2. This property may be useful for designing a novel soliton switching in optics.
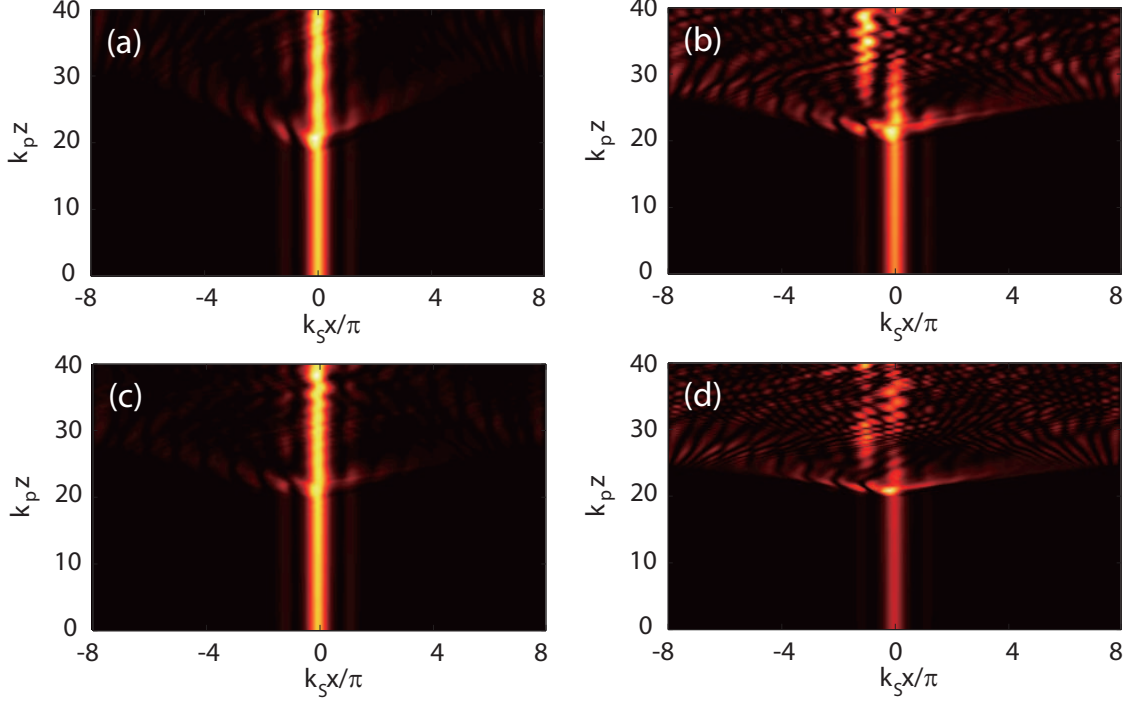
FIG. 5: (Color online) Stability control of the weak-light soliton by changing system parameters W_1, Z_1, and Z_2. (a) The soliton is stable for $(W_1, Z_1, Z_2) = (0.7, 20, 22)$; (b) The soliton is unstable for $(0.8, 20, 22)$; (c) The soliton is stable for $(0.8, 20, 21)$; (d) The soliton is unstable for $(1.6, 20, 21)$.

V. WEAK-LIGHT SOLITONS IN 2D $\mathcal{PT}$-SYMMETRIC POTENTIAL

Because Eqs. (7) can be easily extended into two-dimensional case by taking $\xi \to (\xi, \eta)$ with $\eta = k_S y$, i.e.

$$i\frac{k_p^2}{k_S^2}\frac{\partial \Omega_p}{\partial \zeta} + \frac{1}{2}\left(\frac{\partial^2}{\partial \xi^2} + \frac{\partial^2}{\partial \eta^2}\right)\Omega_p + \frac{k_p^2}{2k_S^2}\chi_p(\xi, \eta)\Omega_p = 0, \qquad (19)$$

where $\chi_p(\xi, \eta)$ has the same expression as before and its dependence on η can be obtained by choosing $\Omega_c = \Omega_c(\xi, \eta)$ and $E_S = E_S(\xi, \eta)$. Then Eq. (8) is changed into

$$\left(\frac{\partial^2}{\partial \xi^2} + \frac{\partial^2}{\partial \eta^2}\right)u + V(\xi, \eta)u + G(\xi, \eta)|u|^2 u = \beta u, \qquad (20)$$

where the ξ- and η-dependence of G is very weak and hence can be neglected.

As a particular case, we consider the 2D periodic $\mathcal{PT}$-symmetric potential with the form

$$V(\xi, \eta) = V_0[\cos^2(\xi) + \cos^2(\eta)] + iW_0[\sin(2\xi) + \sin(2\eta)]. \qquad (21)$$

The corresponding first-order susceptibility of the probe field is

$$\chi_{p,1}(\xi, \eta) = 0.460 - 10^{-3}\{V_0[\cos^2(\xi) + \cos^2(\eta)] + iW_0[\sin(2\xi) + \sin(2\eta)]\}, \qquad (22)$$
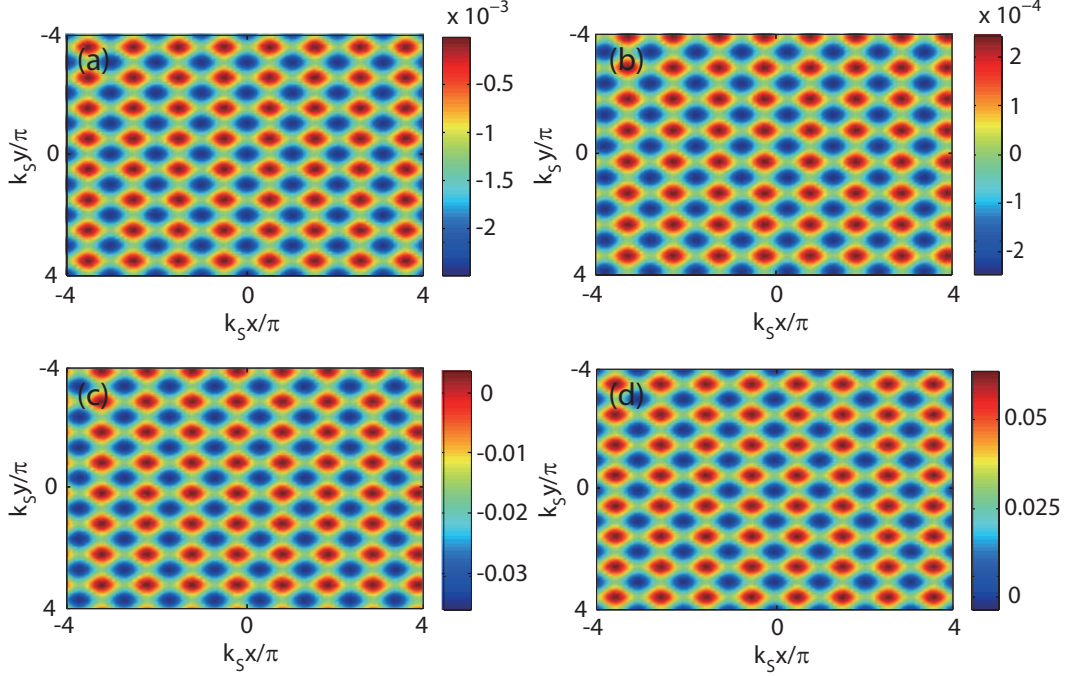
FIG. 6: (Color online) (a) Real part and (b) imaginary part of the 2D $\mathcal{PT}$-symmetric refractive index $n - 1.208$ as a function of $\xi \equiv k_S x/\pi$ and $\eta \equiv k_S y/\pi$ for $V_0 = 3.0$ and $W_0 = 0.75$. (c) The transverse distribution of the control field, $[\Omega_c(\xi) - 2.55]/\Gamma$, required for the refractive index. (d) The transverse distribution of the Stark field, $[E_S(\xi) - 0.97]/E_0$, required for the refractive index.

which can be realized by using the control and Stark fields shaped as

$$\Omega_c(\xi, \eta)/\Gamma \approx 2.553 - 0.002V_0[\sin^2(\xi) + \sin^2(\eta)] - 0.032W_0[\sin(2\xi) + \sin(2\eta)], \quad (23)$$

$$E_S(\xi, \eta)/E_0 \approx 0.97 + 0.008V_0[\sin^2(\xi) + \sin^2(\eta)] + 0.021W_0[\sin(2\xi) + \sin(2\eta)]. \quad (24)$$

Fig. 6(a) (Fig. 6(b)) shows the real (imaginary) part of the 2D $\mathcal{PT}$-symmetric refractive index n as a function of $\xi \equiv k_S x/\pi$ and $\eta \equiv k_S y/\pi$ for $V_0 = 3.0$ and $W_0 = 0.75$, which is below the $\mathcal{PT}$ phase transition point. The real and imaginary parts of the error function $\nu(\xi, \eta) = n(\xi, \eta) - n^*(-\xi, -\eta)$ are of order of 10^{-7} and 10^{-6}, respectively. The transverse distributions of the control (Stark) field required for the refractive index is plotted in Fig. 6(c) (Fig. 6(d)).

The associated band-gap structure of the 2D $\mathcal{PT}$ potential (21) as a function of lattice momentum q is shown in Fig. 7 for $V_0 = 3.0$. Panels (a), (b), and (c) give the results of $\text{Re}(\beta)$ for $W_0 = 0.75$ (below the $\mathcal{PT}$ phase transition point), 1.5 (on the $\mathcal{PT}$ phase transition point), and 2.25 (above the $\mathcal{PT}$ phase transition point), respectively. We see that as W_0
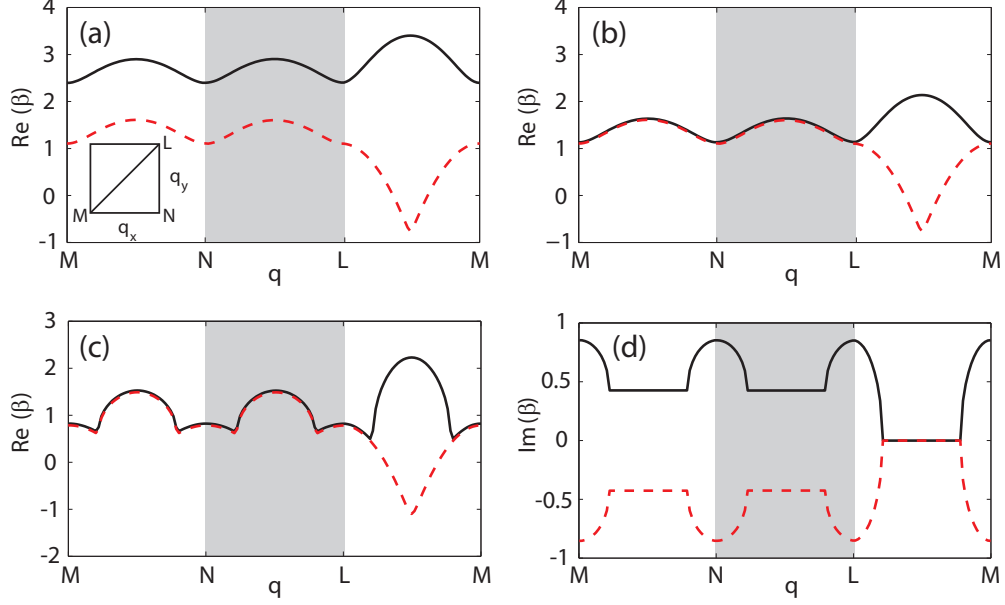
16

FIG. 7: (Color online) Band structure of the 2D $\mathcal{PT}$ potential (21) as a function of lattice momentum q for $V_0 = 3.0$. Shown in (a), (b), and (c) are $\text{Re}(\beta)$ for $W_0 = 0.75$ (a), 1.5 (b), and 2.25 (c), respectively. Points M, N, and L are the corners of the first Brillouin zone, denote $(q_x, q_y) = (-0.5, -0.5)$, $(0.5,-0.5)$, and $(0.5,0.5)$, respectively. (d) $\text{Im}(\beta)$ for $V_0 = 3.0$ and $W_0 = 2.25$, which is zero in the whole (q_x, q_y)-plane for $W_0 = 0.75$ and 1.5.

increases the band gap becomes narrower and closed completely when crossing the critical transition value $W_0/V_0 = 1/2$. The imaginary part of the "energy" band (i.e $\text{Im}(\beta)$) is shown in panel (d) of the figure. One sees that $\text{Im}(\beta)=0$ for $W_0 = 0.75$ and 1.5 in the whole space, but it becomes nonzero for $W_0 = 2.25$.

For obtaining soliton solutions in 2D, Eq. (20) is numerically solved for $W_0/V_0 = 0.25$ (below the $\mathcal{PT}$ phase transition point), for which the corresponding linear eigenvalue equation has a purely real spectrum (i.e. $\text{Im}(\beta) = 0$) located within the first band gap (i.e. $1.1 < \beta < 2.4$). 2D solitons are found, with the result illustrated in Fig. 8. Shown in Fig. 8(a) and Fig. 8(b) are respectively the real part $(\text{Re}(u))$ and imaginary part $(\text{Im}(u))$ of u of a 2D soliton for $\beta = 2.0$ as functions of $k_S x/\pi$ and $k_S y/\pi$. Taking the beam radius ≈ 0.1 mm, the threshold power for generating the 2D soliton is estimated as $P_{\text{th}} \approx 6.9$ nW.

To test the stability of the 2D soliton, the evolution of the 2D soliton is also studied by adding some random noises on both the amplitude and phase to the initial condition of the soliton. The result of numerical simulation is presented in Fig. 8(c) for propagation distance
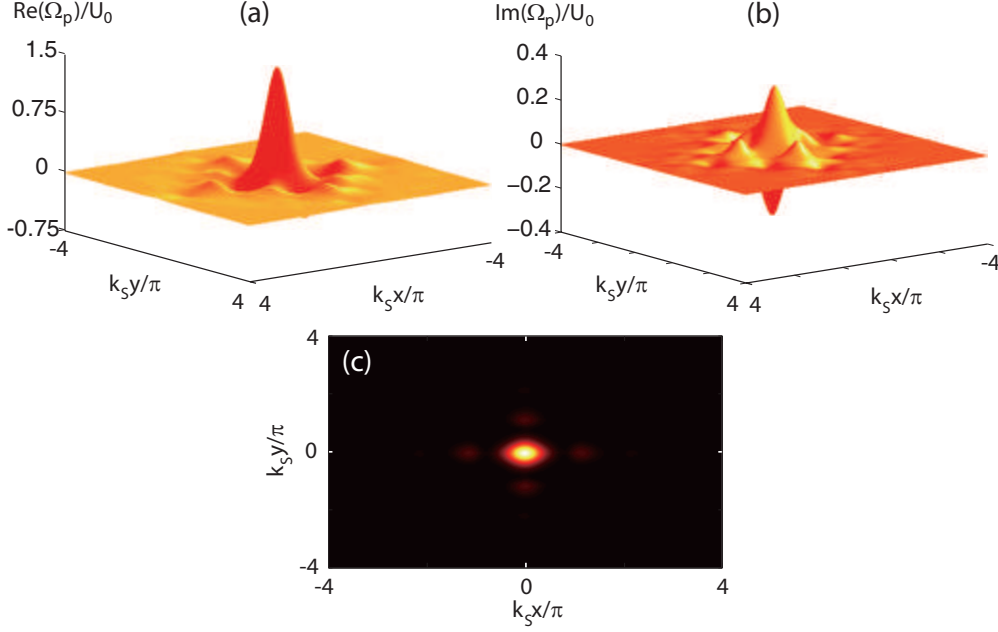
17

FIG. 8: (Color online) Intensity distribution of the weak-light soliton in the 2D $\mathcal{PT}$ system as a function of $k_S x/\pi$ and $k_S y/\pi$. (a) ((b)) The real (imaginary) part of the soliton amplitude $\text{Re}(u)$ ($\text{Im}(u)$) for $\beta = 2$. (c) Light-intensity distribution of the soliton after adding random noises at $k_p z = 40$ on both amplitude and phase to initial condition of the soliton.

up to $z = 40/k_p$. We see that the soliton is fairly stable during propagation. Consequently, stable 2D weak-light solitona are indeed possible in the proposed system.

VI. SUMMARY

In this work, we have proposed a new scheme to generate 1D and 2D weak-light solitons in an atomic system with $\mathcal{PT}$ symmetry. The system we suggest is a cold three-level atomic gas with two species and driven by a control and a probe laser fields. We have shown that by the interference of two Raman resonances highly adjustable probe-field refractive-index with $\mathcal{PT}$ symmetry in 1D and 2D can be realized. We have further shown that it is possible to produce various light solitons when the weak nonlinearity of the probe field is taken into account. Due to resonant character of the system, the light solitons obtained in 1D and 2D have extremely low light power (at the level of nanowatt). In addition, we have demonstrated that the stability of these light solitons can be actively controlled via $\mathcal{PT}$ phase transition of the system. Notice that the scheme we proposed here can be used to realize other types of

refractive indexes, such as the 1D and 2D complex $\mathcal{PT}$-symmetric Scarff II potentials [21]. Our results may have potential applications in the field of optical information at low light level.

Appendix A: Equations for solving $\Omega_c(\xi)$ and $E_{\mathrm{S}}(\xi)$

From the real and imaginary parts of Eqs. (5) and (10), we get the following equations

$$\frac{p_{eg}^2}{\epsilon_0 \hbar}\left(\frac{N_1 \delta_1[\delta_1^2 + \delta_1\Delta_1(\xi) - |\Omega_c(\xi)|^2]}{[\delta_1^2 + \delta_1\Delta_1(x) - |\Omega_c(\xi)|^2]^2 + \delta_1^2\Gamma^2} + \frac{N_2\Delta_2(\xi)}{\Delta_2(\xi)^2 + \Gamma^2}\right) = 0.46 - 10^{-3}V_0\cos^2(\xi) \quad \text{(A1a)}$$

$$\frac{p_{eg}^2}{\epsilon_0 \hbar}\left(\frac{N_1 \delta_1^2\Gamma}{[\delta_1^2 + \delta_1\Delta_1(x) - |\Omega_c(\xi)|^2]^2 + \delta_1^2\Gamma^2} - \frac{N_2\Gamma}{\Delta_2(\xi)^2 + \Gamma^2}\right) = -10^{-3}W_0\sin(2\xi), \quad \text{(A1b)}$$

with $\Delta_s(\xi) = \Delta_s - (\alpha_e - \alpha_g)E_{\mathrm{S}}^2(\xi)/(4\hbar)$. Notice that at $\xi = 0$ the susceptibility must be real, we obtain

$$\frac{N_2}{N_1} = \frac{\delta_1^2(\Delta_{20}^2 + \Gamma^2)}{(\delta_1^2 + \delta_1\Delta_{10} - |\Omega_{c0}|^2)^2 + \delta_1^2\Gamma^2}. \quad \text{(A2)}$$

where Δ_{s0} and Ω_{c0} are denoted as values of $\Delta_s(\xi)$ and $\Omega_c(\xi)$ at $\xi = 0$, respectively. Eq. (A2) imposes a relation between N_1 and N_2. The expressions of $\Omega_c(\xi)$ and $E_{\mathrm{S}}(\xi)$ can be solved from Eqs. (A1a) and (A1b), directly.

Acknowledgments

[1] S. Boettcher and C. M. Bender, Phys. Rev. Lett. **80**, 5243 (1998).

[2] Z. Ahmed, Phys. Lett. A **282**, 343 (2001).

[3] C. M. Bender, D. C. Brody, and H. F. Jones, Phys. Rev. Lett. **89**, 270401 (2002).

[4] A. Mostafazadeh, J. Math. Phys. **43**, 205C214 (2002).

[5] K. G. Makris, R. El-Ganainy, D. N. Christodoul ides, and Z. H. Musslimani, Phys. Rev. Lett. **100**, 103904 (2008).

[6] C. E. Rüter, K.G. Makris, R. El-Ganainy, D. N. Christodoulides, M. Segev, and D. Kip, Nat. Phys. **6**, 192 (2010).

[7] A. Guo, G. J. Salamo, D. Duchesne, R. Morandotti, M. Volatier-Ravat, V. Aimez, G. A. Siviloglou, and D. N. Christodoulides, Phys. Rev. Lett. **103**, 093902 (2009).

[8] L. Feng, M. Ayache, J. Huang, Y.-L. Xu, M.-H. Lu, Y.-F. Chen, Y. Fainman, and A. Scherer, Science **333**, 729 (2011).

[9] A. Regensburger, C. Bersch, M.-A. Miri, G. Onishchukov, D. N. Christodoulides, and U. Peschel, Nature (London) **488**, 167 (2012).

[10] X. Luo *et al.*, Phys. Rev. Lett. **110**, 243902 (2013).

[11] C. Hang, G. Huang, and V. V. Konotop, Phys. Rev. Lett. **110**, 083604 (2013).

[12] J. Sheng, M. Miri, D. N. Christodoulides, and M. Xiao, Phys. Rev. A **88**, 041803(R) (2013).

[13] H.-j. Li, J. Dou, and G. Huang, Opt. Expr. **21**, 32053 (2013).

[14] C. Hang, D. A. Zezyulin, V. V. Konotop, and G. Huang, Opt. Lett. **38**, 4033 (2013).

[15] C. Hang, D. A. Zezyulin, G. Huang, V. V. Konotop, and B. A. Malomed, Opt. Lett. **39**, 5387 (2014).

[16] B. Peng *et al.*, Nat. Phys. **10**, 394 (2014).

[17] L. Chang *et al.*, Nat. Photon. **8**, 524 (2014).

[18] S. Longhi, Phys. Rev. A **82**, 031801(R) (2010).

[19] Z. Lin, H. Ramezani, T. Eichelkraut, T. Kottos, H. Cao, and D. Christodoulides, Phys. Rev. Lett. **106** 213901 (2011).

[20] X. Zhu, L. Feng, P. Zhang, X. Yin, and X. Zhang, Opt. Lett. **38**, 2821C2824 (2013).

[21] Z. H. Musslimani, K. G. Makris, R. El-Ganainy, and D. N. Christodoulides, Phys. Rev. Lett. **100**, 030402 (2008).

[22] H. Wang and J. Wang, Opt. Expr. **19**, 4030 (2011).

[23] Z. Lu and Z. Zhang, Opt. Expr. **19**, 11457C11462 (2011).

[24] F. Kh. Abdullaev, Y. V. Kartashov, V. V. Konotop, and D. A. Zezyulin, Phys. Rev. A **83**, 041805(R) (2011).

[25] Z. Shi, X. Jiang, X. Zhu, and H. Li, Phys. Rev. A **84**, 053855 (2011).

[26] D. A. Zezyulin, Y. V. Kartashov, V. V. Konotop, Europhys. Lett. **96**, 64003 (2011).

[27] Y. He, X. Zhu, D. Mihalache, J. Liu, and Z. Chen, Phys. Rev. A, **85**, 013831 (2012).

[28] S. Nixon, L. Ge, and J. Yang, Phys. Rev. A **85**, 023822 (2012).

[29] V. Achilleos, P. G. Kevrekidis, D. J. Frantzeskakis, and R. Carretero-González, Phys. Rev. A **86**, 013808 (2012).

[30] M. Miri, A. B. Aceves, T. Kottos, V. Kovanis, and D. N. Christodoulides, Phys. Rev. A **86**, 033801 (2012).

[31] C. Huang, C. Li, and L. Dong, Opt. Expr. **21**, 3917C3925 (2013).

[32] R. Driben and B. A. Malomed, Opt. Lett. **36**, 4323C4325 (2011).

[33] N. V. Alexeeva, I. V. Barashenkov, A. A. Sukhorukov, and Y. S. Kivshar, Phys. Rev. A **85**, 063837 (2012).

[34] F. C. Moreira, F. Kh. Abdullaev, V. V. Konotop and A. V. Yulin, Phys. Rev. A **86**, 053815 (2012).

[35] V. V. Konotop, D. E. Pelinovsky and D. A. Zezyulin, Euro. Phys. Lett. **100**, 56006 (2012).

[36] D. A. Zezyulin, V. V. Konotop, and F. K. Abdullaev, Opt. Lett. **37**, 3930C3932 (2012).

[37] Y. V. Kartashov, Opt. Lett. **38**, 2600 (2013).

[38] C. W. Gardiner and P. Zoller, *Quantum Noise* (Second Enlarged Edition) (Springer, Berlin, 2000).

[39] D. Steck, ^{87}Rb and ^{85}Rb D Line Data, http://steck.us/alkalidata.

[40] Y. Bai, N. Bandyopadhayay, S. Tsao, S. Slivken, and M. Razeghi, Appl. Phys. Lett. **98**, 181102 (2011).

[41] A. Lyakh, R. Maulini, A. Tsekoun, R. Go, and C. K. N. Patel, Opt. Express **20**, 4382 (2012).

[42] V. A. Brazhnyi and V. V. Konotop, Mod. Phys. Lett. B **18**, 627 (2004).